Eur.Phys.J. E **14**, 311 (2004)

Mechanical Properties of Mono-domain Side Chain Nematic Elastomers*

PHILIPPE MARTINOTY[1], PASCAL STEIN[1], HEINO FINKELMANN[2], HARALD PLEINER[3], AND HELMUT R. BRAND[4]

1 LDFC, Université Louis Pasteur, 4 rue Blaise Pascal, 67070 Strasbourg, France

2 Institut für Makromolekulare Chemie, Stephan-Meier-Str. 31, 79104 Freiburg, F.R. Germany.

3 Max-Planck-Institut für Polymerforschung, Postfach 3148, 55021 Mainz, F.R. Germany

4 Theoretische Physik III, Universität Bayreuth, 95440 Bayreuth, Germany.

PACS. *83.80.Va Elastomeric polymers – 61.30.v Liquid crystals –83.60.Bc Linear viscoelasticity*

Shortened version of the title: P. Martinoty et al.: Mechanical Properties of Mono-domain SCNE

Abstract. We investigate the behavior of the shear rigidity modulus $G = G' + iG''$ of three mono-domain side chain liquid crystalline elastomers composed of side-chain polysiloxanes cross-linked by either flexible or rigid cross-linkers. The measurements were taken in a frequency domain ranging form $\sim 0.02 Hz$ to $\sim 10^4 Hz$ applying the shear in a plane perpendicular to or containing the director. The measurements as a function of temperature show an anisotropy of G' which appears around T_{NI}, when decreasing the temperature, and which is due to the expected lowering of $G'_{//}$ coming from the coupling between the shear and the director. The measurements as a function of frequency show that G has two components for both geometries, in both the isotropic phase and in the nematic phase around the phase transition. One reflects the network behavior in its hydrodynamic regime (G' is constant and $G'' \sim f$ where f is the frequency), the other which appears at higher frequencies is characterized by a scaling law behavior ($G' \sim G'' \sim f^{0.5}$) of the Rouse type. We discuss the results in the framework of available theories and show that the three elastomers present a non-soft behavior, even for the elastomer for which the contrary was claimed, and that there is no separation of time scales between the director and the network. We also present data on a polydomain sample and a non-mesomorphic one which complement these results.

* Presented at the First World Congress on Biomimetics and Artificial Muscles, 9-11 December 2002, Albuquerque, New Mexico, U.S.A.. Some aspects of this work have been published as an abridged version in the Proceedings of the Conference.

1. Introduction and motivation

Liquid crystal elastomers have been the object of growing interest over recent years, because they constitute a new class of materials, combining the elastic properties of conventional elastomers and the orientational properties of liquid crystals. They are obtained by chemically linking liquid crystal polymer chains by means of a crosslinking agent. The mesogenic groups can be either macroscopically disordered (poly- domain sample) or macroscopically ordered (mono-domain sample) in the liquid crystalline state.

The elastic response of these materials has been studied theoretically, starting from the de Gennes theory [1], which introduces new terms in the free energy coupling the director rotations to the permanent network. The concept of soft elasticity, introduced by Lubensky and Golubovic [2] to define the ability of some materials to change their shape without energy cost, has been applied to liquid crystalline elastomers by Olmsted [3] and Warner, Bladon and Terentjev [4].

In contrast to their elastic properties, their dynamic properties have been much less studied theoretically. Very recently, a viscoelastic theory has been developed by Terentjev and Warner [5, 6]. This theory is based on the linear elasticity of a network in its low-frequency limit, and on an independent relaxation of the director. The essential part of the description is the separation of time scales. It is assumed that the relaxation time of the director ($\tau_n \sim 10^{-2} s$) is much greater than the time scale of the network which is of the order of the Rouse time ($\tau_R \sim 10^{-6} s$). This theory makes predictions about the behavior of the complex shear modulus G as a function of frequency. In the case where the director **n** is perpendicular to the shear velocity (**n** $\perp$ **v**), the theory predicts that G shows the conventional behavior of a rubber with a frequency-independent G' for $\omega < \tau_R^{-1}$. When **n** is parallel to the shear velocity (**n** // **v**), the theory predicts the existence of two rubbery plateaus for G'. One corresponds to the hydrodynamic limit and appears for $\omega < \tau_n^{-1}$, and the other occurs for $\tau_n^{-1} < \omega < \tau_R^{-1}$. The latter one is a consequence of the separation of the time scales evoked above, and of the step of G' associated with the director relaxation. If the concept of soft elasticity is introduced, G' goes to zero in the hydrodynamic limit [5,6]. Terentjev and Warner have also introduced the notion of semi-soft elasticity for non-ideal materials [5]. In that case G' goes to a non-zero but small value in the hydrodynamic limit.

Recently, the dynamic mechanical investigation of mono-domain nematic elastomers has started [6-9] concentrating on the application of simple shear in two different geometries. In one geometry - for **n** perpendicular to the shear velocity ($\mathbf{n} \perp \mathbf{v}$) - there is no coupling between the director **n** and the network, while for **n** parallel to the shear velocity ($\mathbf{n} // \mathbf{v}$), the dynamics of the network is influenced by the existence of the director as evidenced by the observation of a dip in the dynamic shear modulus $G'(\omega)$ as a function of temperature. In refs. [6, 8, 9] it was argued that this dip is due to soft elasticity and that there is a separation of time scales by several orders of magnitude between the relaxation of the director and that of the network.

In this paper we have investigated three different mono-domain samples including one which has the same chemical composition as the samples studied in ref. [6], as well as a poly-domain sample and, for comparison, a non-mesomorphic sample.

This study allowed us to tackle the three fundamental problems raised by these materials; the mechanical anisotropy, the concept of 'soft elasticity', and the possible separation in the time scales between the director relaxation and the network relaxation. Our results show that G' measured for **n** parallel to the shear velocity ($\mathbf{n} // \mathbf{v}$) does not go to zero in the hydrodynamic regime, and that there is no separation in the time scales between the director relaxation and the network relaxation in the non-hydrodynamic regime. Both results are incompatible with the assumptions of Terentjev and Warner [5, 6]. Rather our results, together with those of ref. [6, 8, 9] are compatible with a) the classical hydrodynamic description of nematic elastomers (i.e. the description without soft or semi-soft elasticity) for the data in the hydrodynamic limit, b) $\tau_n \sim \tau_R \sim 10^{-2}$ s, and c) the dynamics of a network having a cascade of Rouse-like modes leading to an $\omega^{0.5}$ response for $\omega \tau_R \gg 1$.

2. The samples: synthesis and characterization

The different elastomers we investigated have been synthesized in the Institut für Makromolekulare Chemie, Freiburg, using the method described in [11]. Samples 1 - 3 are mono-domain nematic elastomers, while sample 4 is a non-mesomorphic elastomer. Sample 5 is the polydomain analogue of sample 2.

Samples 1 and 2 have the same mesogenic groups with the same spacer lengths, but the cross-linkers are different. Sample 1 has flexible cross-linkers, whereas sample 2 has two types of cross-linkers: the flexible one of sample 1, and a rigid one. Sample 3 differs from sample 2 only by the length of the spacers of the mesogenic groups. Sample 4 differs from sample 2 only by the pending side-group, which is non-mesomorphic. The chemical composition is summarized in Figs.1a and 1b.

Figure 1

All samples have 90% of mesogenic groups and 10% cross-linkers (for samples 2 - 5: 6% and 4% of flexible and rigid cross-linkers, respectively). Sample 1 has been studied in detail by the Cambridge group [6, 8, 9] and is considered to be the prototype sample showing soft elasticity. The results for sample 3 have been published in ref. 7.

All samples were characterized by differential scanning calorimetry (DSC) and x-ray scattering. DSC measurements were performed using a Perkin Elmer DSC 7 with cooling rates of 9, 10, 26 and $36 K/min$. The phase transition temperatures were determined by extrapolating to cooling rate zero, and are given in Table I. The decrease in T_{NI} when the length of the spacers is reduced from four methylene groups to three methylene groups is due to the odd-even effect.

The x-ray scattering measurements were performed using a Cu x-ray tube coupled with a graphite monochromator and a $0.5mm$ collimator. The intensity of the scattered x-ray beam was detected by an image plate system. From these experiments, the orientational order parameter was estimated to be ~ 0.7 at room temperature for the three mono-domain elastomers investigated.

The variations in sample-length have been measured as a function of temperature for the three mono-domain elastomers. This change in length is of the order of 60% for sample 2, 40% for sample 1, and 25% for sample 3.

3. Experimental set-up

The complex shear rigidity modulus was measured as a function of frequency and temperature using the piezo-rheometer used previously for studying the rheological properties of elastomers [7, 12-15] and polymers [16, 17]. The principle of the set-up consists in applying a very small shear strain $\leq 10^{-4}$ to the

sample by means of a piezo ceramic vibrating in the shear mode and measuring the shear stress transmitted through the sample using a second piezo ceramic. The strain imposed on the sample is given by

$$\varepsilon = \delta / L \sim V_{in} = (V_0)_{in} exp(i\omega t) \qquad (1)$$

where V_{in} is the voltage applied to the emitting ceramic, δ the shear displacement, and L the sample thickness. The stress measured on the receiving ceramic is given by

$$\sigma = F / S \sim V_{out} = (V_0)_{out} exp(i[\omega t + \phi]) \qquad (2)$$

where F is the force transmitted by the sample, S the sample surface and V_{out} the voltage given by the ceramic. The complex shear rigidity modulus G is given by the stress/strain ratio

$$G = \sigma / \varepsilon \qquad (3)$$

Measurements of G enable the nature and the mechanical properties of the compound to be determined. The phase change ϕ can vary from zero (perfectly elastic solid) to $\pi / 2$ (Newtonian liquid), and is related to the real part G' and the imaginary part G'' of G through the equation

$$tan\phi = G''/G' \qquad (4)$$

In practice, the sample is placed between two glass slides, each of which is stuck to one of the ceramics. The parallelism of the glass slides is adjusted by optical interference measurements to within $\sim 10^{-4} rad$. All the experiments described in this paper were carried out using the same experimental procedure: the sample was placed in the cell at room temperature. The measurements were made between $\sim 18°C$ and $\sim -20°C$, and then between $\sim 18°C$ and $\sim 120°C$ after an annealing time of 45 min at each temperature of measurement. One of the fundamental characteristics of the mono-domain side-chain elastomers is that they spontaneously change their dimensions at the NI-transition. This change in behavior is linked to a variation in length of the elastomer in the direction of the director, which comes from the fact that the mesogens orient themselves in the nematic phase. However, the elastomers stick to the sample-bearing slides, which prevents this change. This frustration effect gives rise to an internal stress which could modify the sample response. The possible influence of this constraint has

been checked by preheating the sample to high temperatures ($\sim 120°C$), placing it into the cell (also heated to $\sim 120°C$) and taking the measurements this time by decreasing the temperature. The results obtained show that the values of G' have slightly changed, but not the value of the dip. This indicates that the nematic director rotation is not strongly impeded by internal constraints, and that therefore the characteristic mechanical properties of the compound are not masked.

The applied strain was $\varepsilon \sim 10^{-4}$ and the validity of the linear response checked experimentally. The sensitivity of the set-up does not allow G'' values of less than $10^3 Pa$ to be measured. G' and G'' were determined to within 10% for values around $10^3 Pa$. The accuracy increases for increasing values of G' and G'' can be estimated to be around $\sim 1\%$ for values higher than $10^4 Pa$. Due to the planar orientation of the director within the film, it was possible to conduct experiments applying the shear parallel or perpendicular to the director and to determine $G_{//}$ and $G_{\perp}$.

4. Theoretical overview

We first present the static continuum description pioneered by P.G. de Gennes [1] and generalized in ref. [10] to incorporate the effect of external fields and dynamic aspects.

Using the notation of ref. [1], the generalized energy associated with the director and the elastic degrees of freedom is assumed to be written as the sum of three contributions:

$$E_g = E_e + E_n + E_{en} \qquad (5)$$

- E_e is the conventional elastic energy for a uniaxial solid

$$\begin{aligned} E_e = {} & \frac{c_{11}}{2}(e_{xx}^2 + e_{yy}^2) + c_{12} e_{xx} e_{yy} + c_{13} e_{zz}(e_{xx} + e_{yy}) \\ & + \frac{c_{33}}{2} e_{zz}^2 + 2c_{44}(e_{yz}^2 + e_{xz}^2) + 2(c_{11} - c_{12}) e_{xy}^2 \end{aligned} \qquad (6)$$

where c_{ij} are the elastic constants.

- E_n is the elastic energy for the director

$$E_n = \frac{K_1}{2}\left(\frac{\partial n_x}{\partial x} + \frac{\partial n_y}{\partial y}\right)^2 + \frac{K_2}{2}\left(\frac{\partial n_x}{\partial y} - \frac{\partial n_y}{\partial x}\right)^2 + \frac{K_3}{2}\left[\left(\frac{\partial n_x}{\partial z}\right)^2 + \left(\frac{\partial n_y}{\partial z}\right)^2\right] \qquad (7)$$

where K_1, K_2, K_3 are the Franck elastic constants [18].

- E_{en} is a coupling energy

$$E_{en} = \frac{D_1}{2}\left[(\Omega_x - \omega_x)^2 + (\Omega_y - \omega_y)^2\right] + D_2\left[(\Omega_y - \omega_y)e_{xz} + (\Omega_x - \omega_x)e_{yz}\right] \qquad (8)$$

where D_1 and D_2 are the coupling constants associated with the relative rotations of the director with respect to the network (D_1) and with the coupling of relative rotations (D_2) to the strain, respectively.

In writing down these equations, we have introduced the linearized strain tensor

$$e_{ij} = \frac{1}{2}\left(\frac{\partial u_i}{\partial x_j} + \frac{\partial u_i}{\partial x_j}\right) \qquad (9)$$

and the rotations

$$\omega_i = \frac{1}{2}\varepsilon_{ijk}\partial_j u_k \qquad (10)$$

with the displacement field u_i. For the director rotations we have

$$\mathbf{\Omega} = \mathbf{n} \times \delta\mathbf{n} \qquad (11)$$

and thus for the relative rotations between the network and the director $\mathbf{\Omega} - \boldsymbol{\omega}$. To be specific we have chosen the uniaxial direction to be parallel to $\hat{z}$.

Now we discuss the two specific shear configurations of interest in analyzing our experimental results in the following. When an homogeneous shear is applied in the plane perpendicular to the director we have for the associated elastic energy, taking into account that only $e_{xy} = e_{yx} \neq 0$,

$$E_g = 2(c_{11} - c_{12})e_{xy}^2 \qquad (12)$$

and thus for the hydrodynamic value of $G'_\perp$

$$G'_\perp = 4(c_{11} - c_{12}) \qquad (13)$$

This result shows that there is for the perpendicular geometry no coupling between the director and the network.

For the parallel geometry for which the director lies in the shear plane, which we have chosen to be the $x-z$ plane, we have for the generalized energy E_g (with $e_{zx} = e_{xz} = \omega_y$)

$$E_g = 2c_{44}e_{xz}^2 + \frac{1}{2}D_1\left(\Omega_y - \omega_y\right)^2 + D_2\left(\Omega_y - \omega_y\right)e_{xz} \qquad (14)$$

Minimizing E_g with respect to $\Omega_y - \omega_y$ and inserting the result into E_g we have

$$E_g = 2\left(c_{44} - \frac{D_2^2}{4D_1}\right)e_{xz}^2 \qquad (15)$$

This result clearly shows that the effective elastic modulus for shear in the plane containing the director is reflecting the coupling of the network and the director rotations leading to a reduction of the shear modulus c_{44} by the amount $\frac{D_2^2}{4D_1}$. The macroscopic shear modulus $G'_{//}$ is therefore given by:

$$G'_{//} = 4\left(c_{44} - \frac{D_2^2}{4D_1}\right) \qquad (16)$$

The above theory concerns the elastic behavior in the static limit. A continuum theory of linear viscoelastic response of nematic elastomer has been developed by Terentjev and Warner [5, 6]. This theory is based on the linear elasticity of a network in its hydrodynamic regime, and on an independent relaxation of the director. It therefore introduces two time scales: a single relaxation time τ_n for the director, and a characteristic time τ_R for the network. τ_n was estimated to be ~ 10^{-2} s on the basis of light scattering experiments [19], and τ_R ~ 10^{-6} s, of the order of the Rouse time for a flexible polymer. To make a comparison with the results of the previous paragraph, we only present the predicted behavior of G' for the perpendicular and parallel geometries.

For the perpendicular geometry, $G'_{\perp}$ is unchanged by the dynamics of the director, and $G'_{\perp}$ is given by eq.(13), for $\omega \ll \tau_R^{-1}$.

For the parallel geometry, for which there is a director rotation, the real part $G'_{//}$ is modified by the director relaxation. For $\omega \ll \tau_R^{-1}$, $G'_{//}$ is given by [5]

$$G'_{//}(\omega) = 4(c_{44} - \frac{D_2^2}{4D_1}) + \frac{(D_2\gamma_1 - D_1\gamma_2)^2}{D_1\gamma_1^2} \times \frac{(\omega\tau_n)^2}{1+(\omega\tau_n)^2} \qquad (17)$$

where $\tau_n = \gamma_1/D_1$ is the relaxation time of the director. γ_1 and γ_2 are friction coefficients associated with the rotation of the director as in a conventional nematic liquid. Equation 17 shows that $G'_{//}$ is a constant in the hydrodynamic regime ($\omega\tau \ll 1$), then increases because of the relaxation of director, and finally is again a constant in the high-frequency regime ($\omega\tau \gg 1$). The hydrodynamic value is identical to that given by eq. (16). As will be discussed in section 6.4, we observe experimentally no evidence for the high frequency plateau predicted by eq. (17).

We close this section by pointing out that 'soft elasticity' corresponds to the requirement [5, 6]

$$G'_{//}(\omega = 0) = 4(c_{44} - \frac{D_2^2}{4D_1}) \equiv 0 \qquad (18)$$

As underlined by Terentjev and Warner, the hydrodynamic value of $G'_{//}$ is therefore the key parameter for determining whether the material is soft, or semi-soft.

5. Results

5.1. Behavior of $G'_{\perp}$ and $G'_{//}$ as a function of temperature

5.1.1. Perpendicular case

Figure 2a and Fig. 3a show the behavior of $G'_{\perp}$ as a function of temperature for samples 1 and 2, respectively.

In the nematic phase the main part of the response of G' is under the influence of the glass transition, as shown by the continuous decrease of G' for all the frequencies considered when the temperature is increased. In the isotropic

phase the thermal behavior of G' is different depending on whether the experiments are made for low or for high frequencies. At low frequencies ($f < 10Hz$), G' obeys the conventional behavior $G' \sim k_B T$, and consequently increases when the temperature is increased. This can be explained by the fact that the behavior of G' is hydrodynamic at these frequencies, as shown by the phase angle ϕ , which is near zero. For frequencies higher than $10Hz$, G' decreases when the temperature is increased, which shows that G' is still under the influence of the glass transition, as indicated by the phase angle which is now different from zero. The figures show that there are no anomalies at all around the N - I transition. In these curves and the following ones the transition temperatures are those determined by DSC.

Figures 2 and 3

5.1.2. Parallel case

Figure 2b and Fig. 3b show the behavior of G' as a function of temperature for samples 1 and 2, respectively. As for the perpendicular case, it can be seen that the overall behavior is under the influence of the glass transition, with, in addition, an anomaly which appears around the nematic to isotropic phase transition. This anomaly is more marked at low frequency when the response of the sample is hydrodynamic. It progressively decreases when the frequency is increased, as a result of the effects associated with the dynamics of the glass transition which becomes dominant. Because of this anomaly G' becomes anisotropic by entering in the nematic phase. Similar behavior for both, the parallel and perpendicular cases, has been observed for sample 3 [7].

5.1.3. Poly-domain sample

Figure 4 shows the results obtained for the polydomain elastomer (sample 5). The temperature dependence of G' shows the same quantitative behavior as that of its mono-domain analogue (sample 2) in the parallel geometry: a marked influence of the glass transition, and a small anomaly near the $N - I$ transition, because in a polydomain sample there are always domains that are sheared in a direction parallel to the director.

5.1.4. Non-mesomorphic sample

Figure 5 shows the variation of G' as a function of temperature for the non-mesomorphic elastomer (sample 4). The comparison with the results obtained for the nematic samples indicates that the influence of the glass transition on the G' behavior is strongly reduced, with the result that the purely elastic response is observed for temperatures closer to T_G than those associated with the nematic samples. The dynamics of the glass transition is therefore modified by the presence of the nematic order.

5.1.5. Mechanical anisotropy

To better see the anisotropy of the mono-domain samples, we have represented for each frequency the behavior of $G'_{//}$ and $G'_{\perp}$ as a function of temperature on the same figure. A typical example is given by Fig.6 associated with sample 2.

The following observations can be made. Firstly, the results obtained at high temperature show that the shear modulus is isotropic (these are the raw data; there is no vertical shift from one curve to another), and becomes anisotropic when the temperature is reduced. Secondly, the anisotropy already appears in the isotropic phase at temperatures far above the T_{NI} transition. Thirdly the value and the nature of the anisotropy considerably change when the frequency is increased. For example, the anisotropy measured at $T \sim 80°C$ is hydrodynamic in nature at $1Hz$ and becomes more and more viscoelastic when the frequency is increased. At $1000Hz$ all the data are in the viscoelastic regime (the hydrodynamic response is indicated by a straight line on the figure). These effects will be discussed in detail later. To follow the variation of the anisotropy from the isotropic phase to the glassy state, the $G'_{//}/G'_{\perp}$ ratio has been represented as a function of temperature. The data associated with sample 2 are shown in Fig.7.

Figure 7

The results obtained at $1Hz$ show again that the shear modulus is isotropic ($G'_{//}/G'_{\perp}=1$) at high temperatures, but becomes anisotropic when the temperature is decreased. The new point is that the anisotropy changes its sign when the temperature is reduced. Results obtained at $100Hz$ and $1000Hz$ show a similar behavior, but the temperature at which the anisotropy changes its sign increases when the frequency increases. This observation shows, without any ambiguity, that the anisotropy change comes from the dynamics of the glass transition.

5.2. Behavior of G' and G'' as a function of frequency

We shall now consider the behavior of G' and G'' as a function of frequency and we start with Fig.8 showing as an example the results obtained in the isotropic phase for sample 2 at $T=90°C$. It can be seen that G has two components. One corresponds to the network behavior in its hydrodynamic regime ($G'=G_0+i\omega\eta$). The other which appears at frequencies higher than $10^2\,Hz$ is viscoelastic in nature.

Figure 8

The characteristic time of the slowest mode of the network is given by the intersection of the G' and G'' curves associated with the hydrodynamic regime. This time is $10^{-2}\ldots10^{-3}s$ depending on the sample for $T=90°C$, and is thus much longer than the slowest relaxation time of the Rouse modes of a conventional polymer. In this respect, it should be noted that the results obtained on a similar mesogen-free elastomer exhibit a frequency-independent G_0 in all our frequency range, ie. up to $10^4\,Hz$.

Figs. 9a and 10a associated with samples 1 and 2, respectively, show the results obtained in the nematic phase when the samples are sheared in the direction perpendicular to the director, for a temperature corresponding to the maximum value of the anisotropy. One observes the same overall behavior of G' and G'' as previously in the isotropic phase. However, the viscoelastic part is now more developed because the slowest relaxation mode of the network is longer due to the decrease in temperature. Both figures show that G' and G'' follow a scaling

behavior of the Rouse type ($G' \sim G'' \sim f^{0.5}$) for frequencies higher than $10^2 Hz$ (sample 1) and $10^3 Hz$ (sample 2).

Figures 9 and 10

Figs.9b and 10b show the result obtained at the same temperature when the samples are sheared in the plane containing the director. The striking result is that the behavior of the shear modulus is the same as the one observed in Figs.9a and 10a for the perpendicular case, except for the small decrease in the hydrodynamic value of G'. This means that we observe no step associated with the director fluctuations. Their effects can show up in the coefficients of iω in the low frequency expansion of the shear modulus. Fig.11 shows the results obtained more deeply in the nematic phase of sample 2 when the sample is sheared parallel or perpendicular to the director.

Figure 11

Because of the strong increase of the relaxation time of the network the viscoelastic part of the sample response is now fully developed, and confirms it is of the Rouse type. It should be stressed that this important conclusion is directly obtained due to the wide frequency range provided by the set-up, without using the time - temperature superposition assumption.

6. Discussion

6.1. General behavior

All the mono-domain samples studied here show in the hydrodynamic limit the same overall behavior characterized by an anomaly around the NI-transition for the parallel case and no anomaly for the perpendicular case. This change in behavior supports the coupling between the director and the shear introduced by de Gennes for the parallel case [1]. The anomaly is also observed for the polydomain analogue of sample 2, as shown by Fig.4, and also for the polydomain analogues of samples 1 and 3 [20]. Only the polydomain samples studied in ref. [12] have not shown the effect. But, as already remarked in ref. [12], these elastomers are very particular in the sense that the cross-linker length is shorter ($\sim 15 Å$ in the most extended conformation) than the mesogen length ($\sim 24 Å$).

The motion of the mesogens is therefore strongly hampered by the cross-linkers, and this cage effect might explain the absence of an anomaly.

For the three mono-domain samples, the decrease in G' starts at a temperature located well above the NI-transition determined by DSC. This indicated that the samples are 'above' the mechanical critical point predicted by de Gennes [21], due to the stretching of the polymer chains during their synthesis. This means that there is no thermodynamic phase transition at all, but a continuous evolution of the orientational order parameter within a single phase called 'isotropic' at high temperature and 'nematic' at low temperature. Of course, this effect disappears for the polydomain sample, and the dip appears very close to the NI-transition temperature determined by DSC, as shown by Fig.4.

The comparison between the amplitudes of the dips determined for the three mono-domain samples shows that the strength of the coupling between the shear and the director is material-dependent. In particular, the comparison between Fig.7 and Fig.12 of [7] shows that the length of the spacers plays an important role since the reduction from 4 methylene groups (sample 2) to 3 methylene groups (sample 3) leads to a reduction of the hydrodynamic dip by a factor of ~ 2. Note that the influence of the spacer length on the coupling between the network and the liquid crystal phase is also seen in the thermo-elastic measurements [22]. The rigidity of the cross-linkers also affects the coupling, but this effect is small, as expected, as shown by the comparison between the values of the ratio $G'_{\perp}/G'_{//}$, which is of the order of ~ 2.5 for sample 1 (Fig.9) and of the order of ~ 2 for sample 2 (Fig.10). However, the value of the hydrodynamic shear modulus is strongly modified by the rigidity of the cross-linker, as shown by the increase by a factor of ~ 7 of the rigidity modulus of the isotropic phase (see Fig.2 and Fig.3). As a result, the longest relaxation time of the network is also affected since it is $\sim 10^{-2} s$ for sample 1 (Fig. 9a) and $\sim 3\times 10^{-3} s$ for sample 2 (Fig. 10a). These values are obtained by evaluating the intersection point of the hydrodynamic behavior of G' and G''.

A last point concerns the mechanical loss. As can be seen in the insets of Figs.2, 3 and 4, the values of the phase angle ϕ, that describe the internal mechanical loss in the compounds, are comparable for the perpendicular case, the parallel case and the poly-domain case. This highlights that this high internal loss does not arise from the concept of 'dynamic soft elasticity', in contrast to the

claims of refs.[6, 8], but is rather caused by the presence of interacting bulky side groups. In this respect it should be noted that the width in temperature of this large internal mechanical loss is reduced when the bulky side groups are non-mesomorphic as shown by the insert of Fig. 5 associated with the non-mesomorphic sample.

6.2. Mechanical anisotropy and the question of soft elasticity in the hydrodynamic regime

All the mono-domain elastomers studied exhibit a mechanical anisotropy around the NI - transition. In the hydrodynamic limit this anisotropy, which is characterized by the relationship $G'_{//} < G'_{\perp}$, comes from a decrease in $G'_{//}$, which is associated with a coupling between the shear and the director. $G'_{//}$ is not zero, in contrast to 'soft elasticity', and the ratio $G'_{\perp}/G'_{//} \sim 2\ldots3$ for all samples, in contrast to 'semi-soft' elasticity. The fact that $G'_{//}$ is essentially independent of the sample preparation and handling, suggests that the internal constraints present in the compounds do not mask the properties associated with 'soft elasticity'. Our results can be well explained without making use of the soft elasticity concept, since, in the hydrodynamic limit, $G'_{\perp}$ and $G'_{//}$ are given by eqs. (13) and (16) respectively. $G'_{\perp}$ has the expected behavior, because of the absence of a coupling between the director and the shear for this geometry, whereas $G'_{//}$ is renormalized by the coupling term via the contribution $\sim D_2^2/D_1$. Since D_1 is positive, the effect of the renormalization is to decrease $G'_{//}$. Far above the NI – transition $G'_{\perp} = G'_{//}$, which means that $c_{11} - c_{12} = 2c_{44}$. If this relationship is assumed to be valid around the transition, then eq.(16) shows that the dip in $G'_{//}$ essentially comes from the D_2^2/D_1 effect, and the value of the dip gives an estimate of D_2 in terms of D_1. We find for sample 2 at the low temperature limit of the hydrodynamic regime for $1Hz$: $D_2^2/D_1 \approx 5\times10^4\,Pa$.

The increase in $G'_{//}$ and $G'_{\perp}$ observed at a given frequency when the glass transition is approached or when the frequency increases for a given temperature, indicates the existence of relaxation modes that are progressively frozen. The change of sign of the anisotropy shows that the contributions of these modes are

not the same for $G'_{//}$ and $G'_{\perp}$. This can be easily explained by noting that some of them are directly coupled to the shear in the parallel case, via the mesogenic groups, and not in the perpendicular case.

6.3. Rouse modes in classical polymers and their analogue in liquid crystalline side chain elastomers

In the isotropic phase as well as in the nematic phase for both, the parallel and the perpendicular geometries, our results show that the viscoelastic response of the samples is of Rouse-type with G' approximately equal to G'' leading to a ~ 0.5 power-law exponent. Our results also show that the longest relaxation time of the network is much longer ($\tau_n \sim 10^{-2} s$) than the relaxation times of the Rouse modes ($\tau_R \sim 10^{-6} s$) in a conventional polymer. This key difference in behavior between ordinary polymers and liquid crystalline side-chain elastomers can be traced back to the fact that the monomers bear bulky mesogenic side groups. As a consequence there is a dramatic increase of the relaxation times of the Rouse-type modes without a significant modification of the power-law exponent in the frequency regime above the hydrodynamic regime. This dramatic increase of the relaxation times of the network is also in contradiction with the assumption made in refs.5 and 6, that there would be a separation of time scales between the director and the Rouse modes with the director being much slower than the Rouse modes. An inversion of the time scales of relaxation (10^{-2} s for the network and 10^{-6} s for the director) is not an option for at least two reasons: a) the relaxation time of the director must be slower than that observed in a conventional nematic phase, and a time of 10^{-6} s has never been reported for a nematic phase, b) light scattering studies [19], also made on a similar sample as in ref 6, show that the director modes are typically in the 10^{-1} - 10^{-2} s range.

Our results show that the Rouse response is universal for side-chain liquid crystal elastomers and does not depend, to first approximation, on the director orientation with respect to the applied strain. It should be noted that, for a material similar to sample 1, the Cambridge group [9] finds that the viscoelastic part of the master curve describing the sample response is characterized by $G' \approx G''$ and is associated with an exponent 0.65, and not 0.5 as expected from linear response.

The origin of this result could be due to the high value [6] of the applied strain ~ 0.02.

We expect the frequency regime above the hydrodynamic regime to be universal (in the sense that the exponent is around 0.5) for side chain liquid crystal elastomers (SCLCEs) when a mesogenic group is attached on each monomer. This has been observed for all the monodomains or polydomains we have studied (see ref. 7 for the nematic phase, and ref. 14 for the isotropic phase). Samples prepared in a different way, but still having a mesogenic group attached on each monomer, also have the same viscoelastic behavior (see refs. 12 and 15). Deviations appear for samples with non-mesomorphic bulky side groups (see Fig 10 of ref. 7), or when the amount of the grafted mesogenic side-groups is too small to have a nematic phase (see Fig 8 of ref. 15).

In closing this section we compare the rheological response of side chain liquid crystal polymers (SCLCPs) with that of SCLCEs. The experiments carried out in several SCLCPs as a function of sample thickness show that the low frequency response of G' shifts progressively from a liquid type behavior ($G' \sim \omega^2$; $G'' \sim \omega$) for thick samples (≥ 100 μm) to a gel like behavior (G'=cst; $G'' \sim \omega$) for thin samples (< 100μm). This unexpected change in behavior has been explained by the presence of transient elastic clusters of macroscopic size, suggesting that these polymers do not behave like melts but like physical gels [16]. The value of the exponent associated with the frequency regime above the hydrodynamic regime is ~ 0.66. Although the dynamics is not Rouse (the physics is not the same) it can be noted that the slowest relaxation time of the uncrosslinked version of sample 1 (the so called 100% sample in the reference quoted above) is $10^{-2} - 10^{-3}$ s in the nematic phase, which is comparable to that of sample 1.

6.4. The separation of time scales

As already explained above, experiments as a function of frequency are the crucial test to determine whether the time scales are separated or not. We shall examine the behavior in the nematic phase in the temperature range where the mechanical anisotropy is the highest. The results in Fig.9 for sample 1 and Fig.10

for sample 2 show that $G'_{//}$ exhibits the same behavior as $G'_{\perp}$. The step predicted by the Terentjev-Warner theory for $G'_{//}$ is therefore not observed, demonstrating that there is no separation of time scales between the director and the network.

The fact that the mesogens are attached to the network explains why the director relaxation is coupled to the Rouse-type behavior and is therefore not visible independently in the frequency response above the hydrodynamic regime. This is in agreement with the light scattering results [19] which precisely show that the director fluctuations are coupled to the network and exhibit relaxation times in the range of about $10^{-2} \ldots 10^{-1} s$.

Naturally one cannot prove experimentally that a material which exhibits a separation of time scales assumed in refs. 5 and 6 does not exist. We believe that the director relaxation time is comparable to that of the slowest mode of the network. In our spirit, a separation of time scales in SCLCEs cannot arise because the relaxation of the director will be always embedded in the Rouse modes, owing to the fact that each monomer bears a mesogenic group. The fact that the slowest frequency relaxation of the network is also very slow in the isotropic phase shows well that it is the mesogenic bulky side groups which slow down the Rouse modes.

7. Conclusions

In this article, we have studied three major problems associated with side-chain nematic elastomers: the mechanical anisotropy, soft elasticity, and the separation of time scales between the director relaxation and the network relaxation. This study was conducted on a series of nematic elastomers including three different monodomain samples and, for comparison, a polydomain sample and a non-mesomorphic sample. Our results show that the decoupling approximation hypothesized in refs. [5, 6] does not work, and that the measured relaxation time is the slowest relaxation time of the network, as a whole. The ratio $G'/G'_{//}$ is between 2 and 3, clearly showing the non-soft behavior of these systems. Our study shows that the nematic elastomers we investigated together with that studied by the Cambridge group can be described as uniaxial rubber

network with a small mechanical anisotropy in the hydrodynamic regime, and a Rouse-like frequency dependence in the viscoelastic region.

This work was carried out within the framework of a Procope program. We thank the Ministère des Affaires Etrangères (96096) and the Deutscher Akademischer Austauschdienst (312/pro-gg) for support of this project. HRB thanks the Deutsche Forschungsgemeinschaft for partial support of his work through Sonderforschungsbereich 481 ″Komplex Polymer und Hybridmaterialen in inneren und äußeren Feldern″.

References

[1] P.G. de Gennes, p.231, in *Liquid Crystals of One- and Two-Dimensional Order*, W. Helfrich and G. Heppke, Eds., Springer, Berlin, 1980.

[2] L. Golubovic and T.C. Lubensky, *Phys. Rev. Lett.* **63**, 1082 (1989).

[3] P. Olmsted, *J. Phys II France* **4**, 2215 (1994).

[4] M. Warner, P. Bladon, and E.M. Terentjev, *J. Phys II France* **4**, 93 (1994).

[5] E.M. Terentjev and M. Warner, *Eur. Phys. J. E* **4**, 343 (2001).

[6] S.M. Clarke, A.R. Tajbakhsh, E.M. Terentjev and M. Warner, *Phys. Rev. Lett.* **86**, 4044 (2001).

[7] P. Stein, N. Aßfalg, H. Finkelmann and P. Martinoty, *Eur. Phys. J. E* **4**, 255 (2001).

[8] S.M. Clarke, A. Hotta, A.R. Tajbakhsh, and E.M. Terentjev, *Phys. Rev. E* **65**, 021804 (2002).

[9] A. Hotta and E.M. Terentjev, *Eur. Phys. J. E* **10**, 291 (2003).

[10] H.R. Brand and H. Pleiner, *Physica A* **208**, 359 (1994).

[11] J. Küpfer and H. Finkelmann, *Makromol. Chem. Rapid Commun.* **12**, 717 (1991).

[12] J.-L. Gallani, L. Hilliou, P. Martinoty, F. Doublet, and M. Mauzac, *J. Phys II France* **6**, 443 (1996).

[13] J. Weilepp, P. Stein, N. Aßfalg, H. Finkelmann, P. Martinoty, and H.R. Brand, *Eur. Phys. Lett.* **47**, 508 (1999).

[14] J. Weilepp, J.J. Zanna, N. Assfalg, P. Stein, L. Hilliou, M. Mauzac, H, Finkelmann, H.R. Brand, and P. Martinoty, *Macromolecules* **32**, 4566, (1999).

[15] J.J. Zanna, P. Stein, J.D. Marty, M. Mauzac, and P. Martinoty, *Macromolecules* **35**, 5459 (2003).

[16] P. Martinoty, L. Hilliou, M. Mauzac, L. Benguigui and D. Collin, *Macromolecules* **32**, 1746, (1999).

[17] D. Collin and P. Martinoty, *Physica A* **320**, 235 (2003).

[18] See for instance, P.G. de Gennes and J. Prost, *The Physics of Liquid Crystals,* 2nd ed., Oxford, Clarendon Press (1995).

[19] M. Schönstein, W. Stille, and G. Strobl, *Eur. Phys. J. E* **5**, 511 (2001).

[20] unpublished results.

[21] P.G. de Gennes, *Comptes Rend. Acad. Sci. Paris* **B281**, 101 (1975).

[22] A. Greve and H. Finkelmann, *Macromol. Chem. Phys.* **202**, 2926 (2001).

Figure legends

Fig. 1. Chemical structure of the samples. Sample 1: $x = 90\%$, $y = 10\%$; samples 2, 3 and 4 $x = 90\%$, $y = 6\%$, $z = 4\%$.

Fig. 2. Temperature dependence of the shear modulus $G'(T)$ and the phase shift $\varphi(T)$ for sample 1. Panel *a* corresponds to a shear velocity $\mathbf{v}$ perpendicular to the director, and panel *b* to a shear shear velocity $\mathbf{v}$ parallel to the director. The transition temperatures were determined by DSC.

Fig. 3. Same as Figure 2, but for sample 2.

Fig. 4. Temperature dependence of the shear modulus $G'(T)$ and the phase shift $\varphi(T)$ for the polydomain sample 5. The transition temperatures were determined by DSC.

Fig. 5. Same as Figure 4, but for the non-mesomorphic sample 4.

Fig. 6. Temperature dependence of $G'_{//}$ and $G'_{\perp}$ for sample 2, at different frequencies: 1 , 10 , 100 and $1000 Hz$ (from top to bottom). For each panel the straight line indicates the range of hydrodynamic behavior.

Fig. 7. Temperature dependence of the $G'_{//} / G'_{\perp}$ ratio for sample 2 at different frequencies: 1 , 100 and $1000 Hz$ (from top to bottom).

Fig. 8. Behavior of G' and G'' as a function of frequency in the isotropic phase of sample 2. The straight line indicates the hydrodynamic behavior of G''.

Fig. 9. Behavior of G' and G'' as a function of frequency in the nematic phase of sample 1 near the N-I transition. Panel *a* corresponds to a shear velocity $\mathbf{v}$ perpendicular to the director, and panel *b* to a shear velocity $\mathbf{v}$ parallel to the director. The straight lines indicate the hydrodynamic behavior of G''.

Fig. 10. Same as Figure 9, but for sample 2.

Fig. 11. Behavior of G' and G'' as a function of frequency deep in the nematic phase of sample 1 showing that the viscoelastic part of the sample's response is Rouse-like. The curves for $\mathbf{n} \perp \mathbf{v}$ have been shifted vertically by one order of magnitude for clarity.

Tables

Table 1. Transition temperatures of the samples.

sample	$T_G\,(°C)$	$T_{NI}\,(°C)$
1	~ 0	~ 80
2	~ 0	~ 80
3	~ 1	~ 58
4	~ –14	-
5	~ 0	~ 80

a)

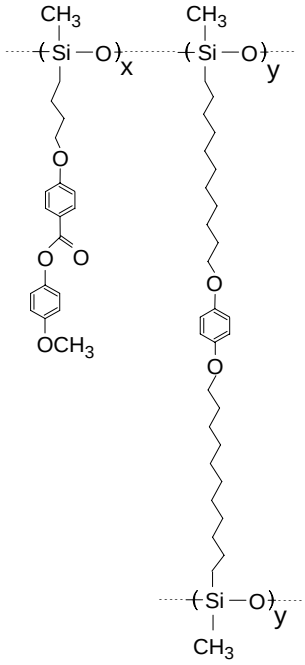

sample 1

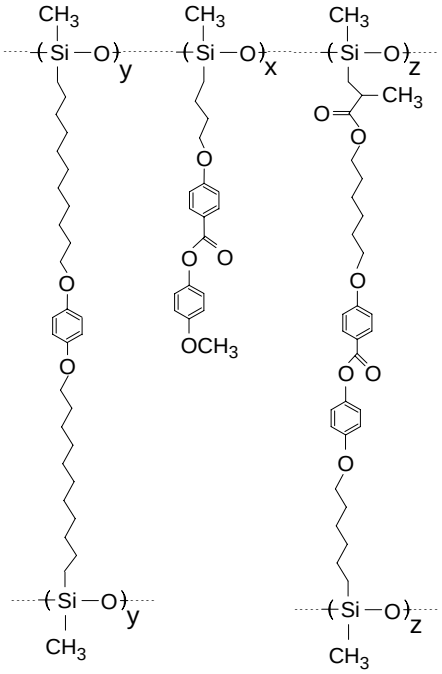

sample 2

b)

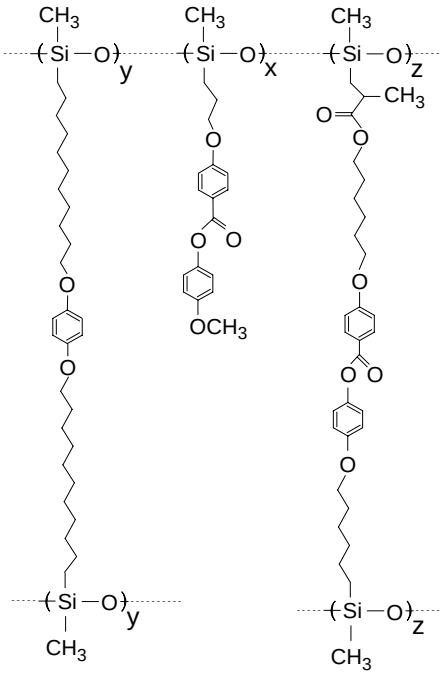

sample 3

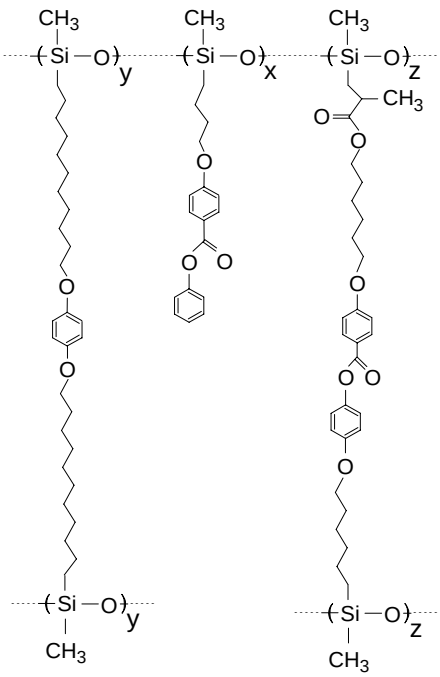

sample 4

Fig. 1

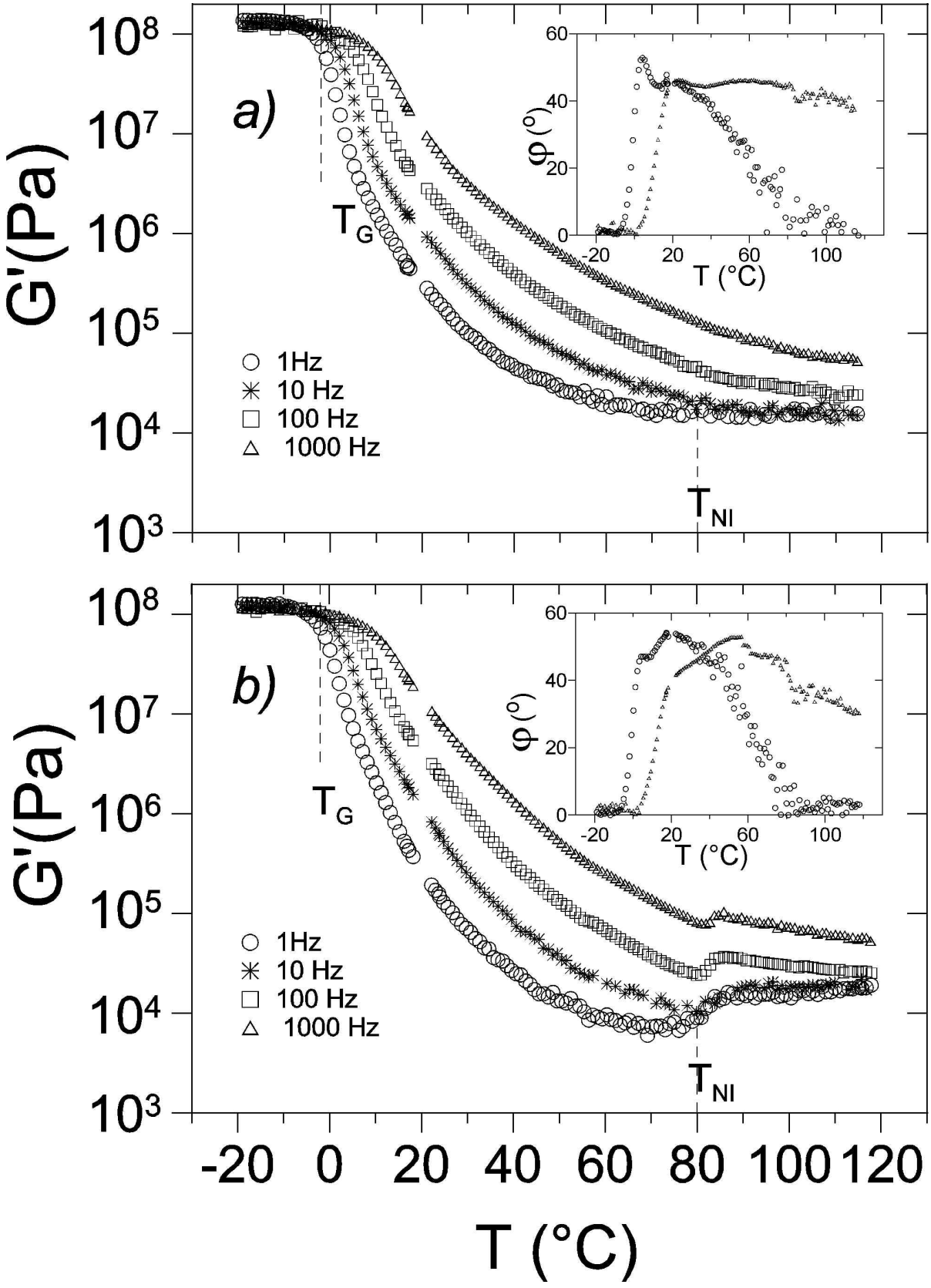

Fig. 2

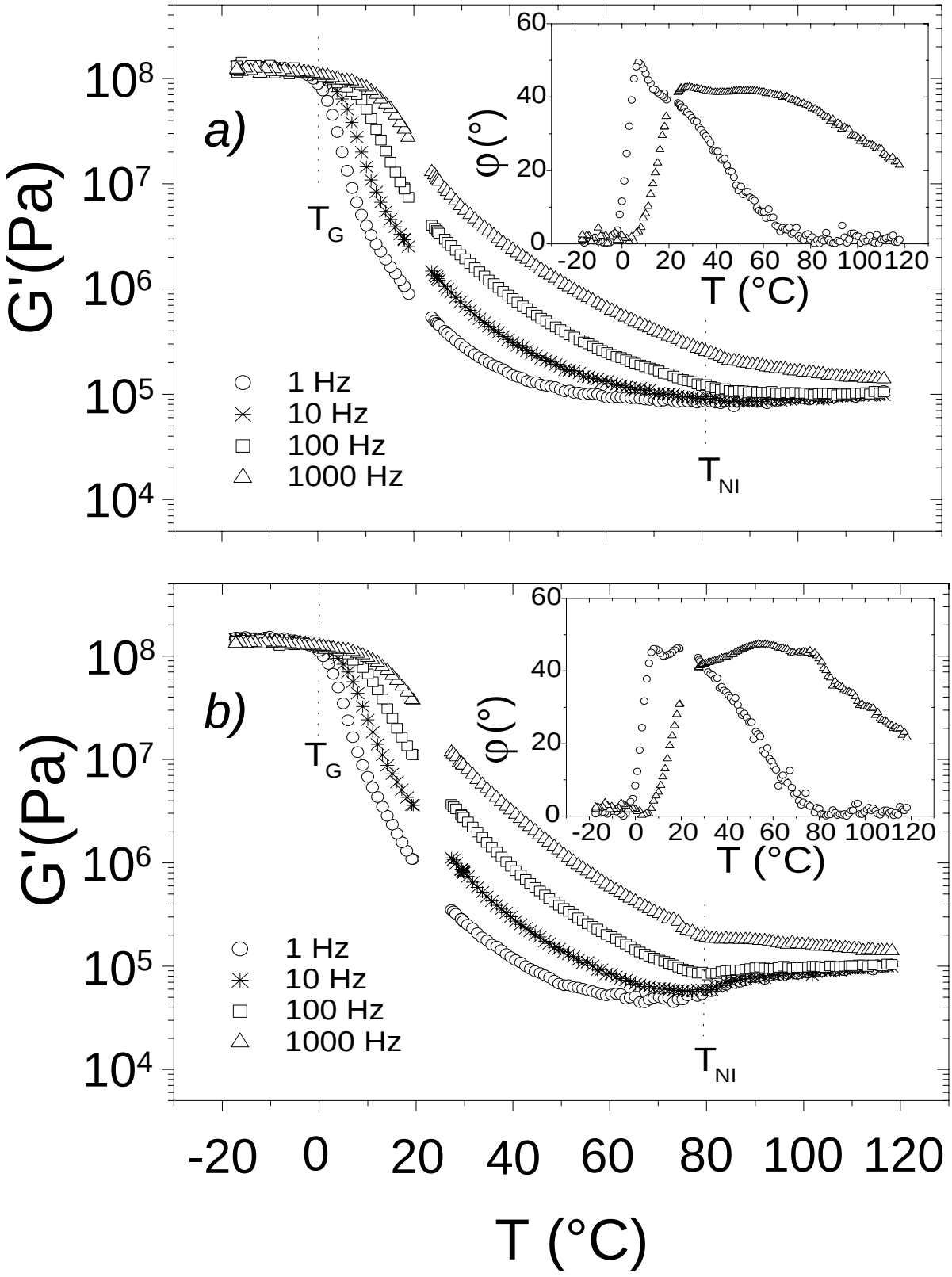
a)
b)
G'(Pa)
10^8
10^7
10^6
10^5
10^4
T_G
T_{NI}
1 Hz
10 Hz
100 Hz
1000 Hz
φ (°)
60
40
20
0
-20 0 20 40 60 80 100 120
T (°C)

Fig. 3

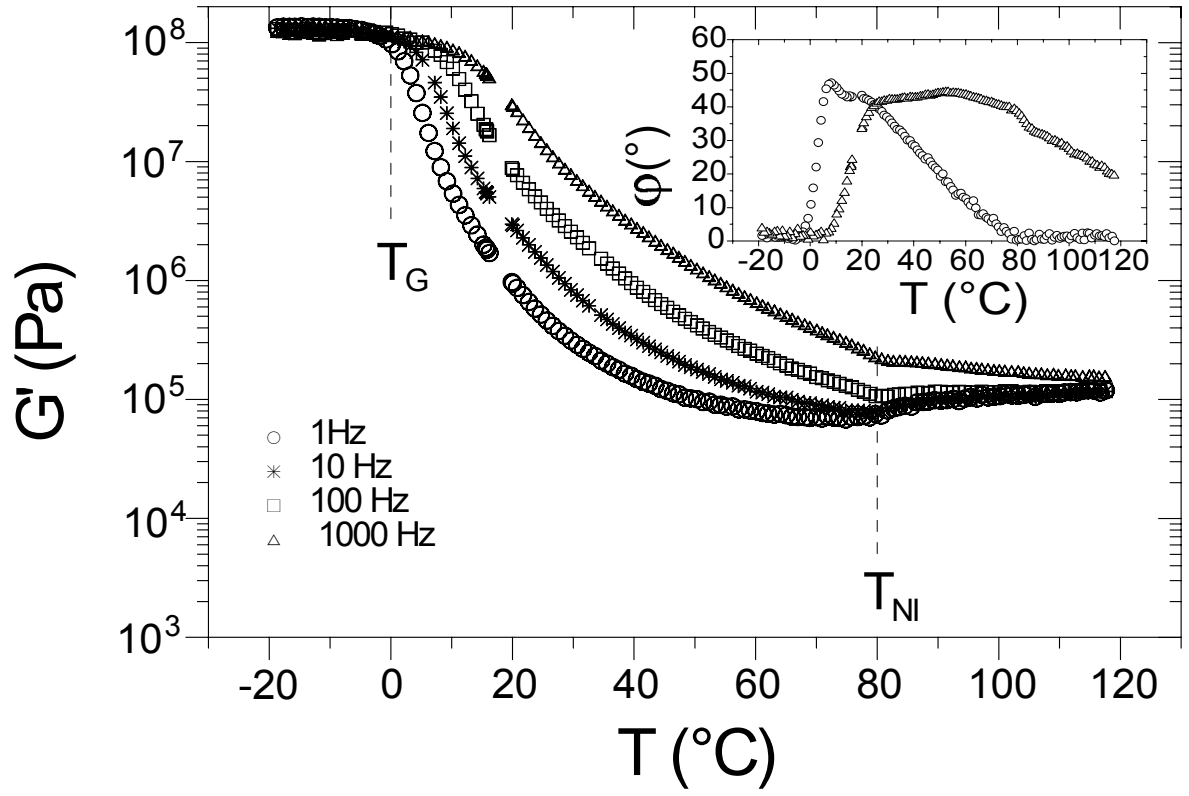
G' (Pa)
T (°C)
T_G
T_NI
1Hz
10 Hz
100 Hz
1000 Hz
φ(°)

Fig.4

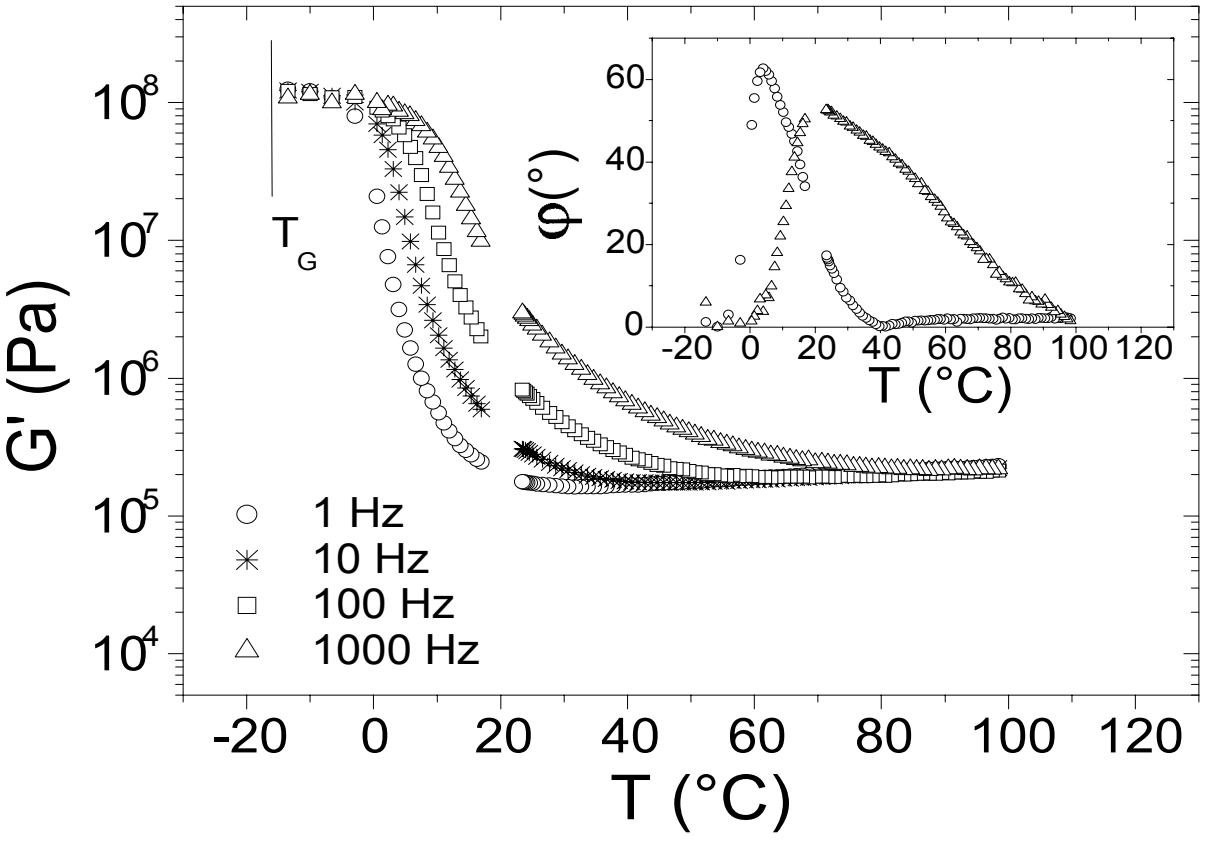
G' (Pa)
T (°C)
T_G
1 Hz
10 Hz
100 Hz
1000 Hz
φ(°)

Fig. 5

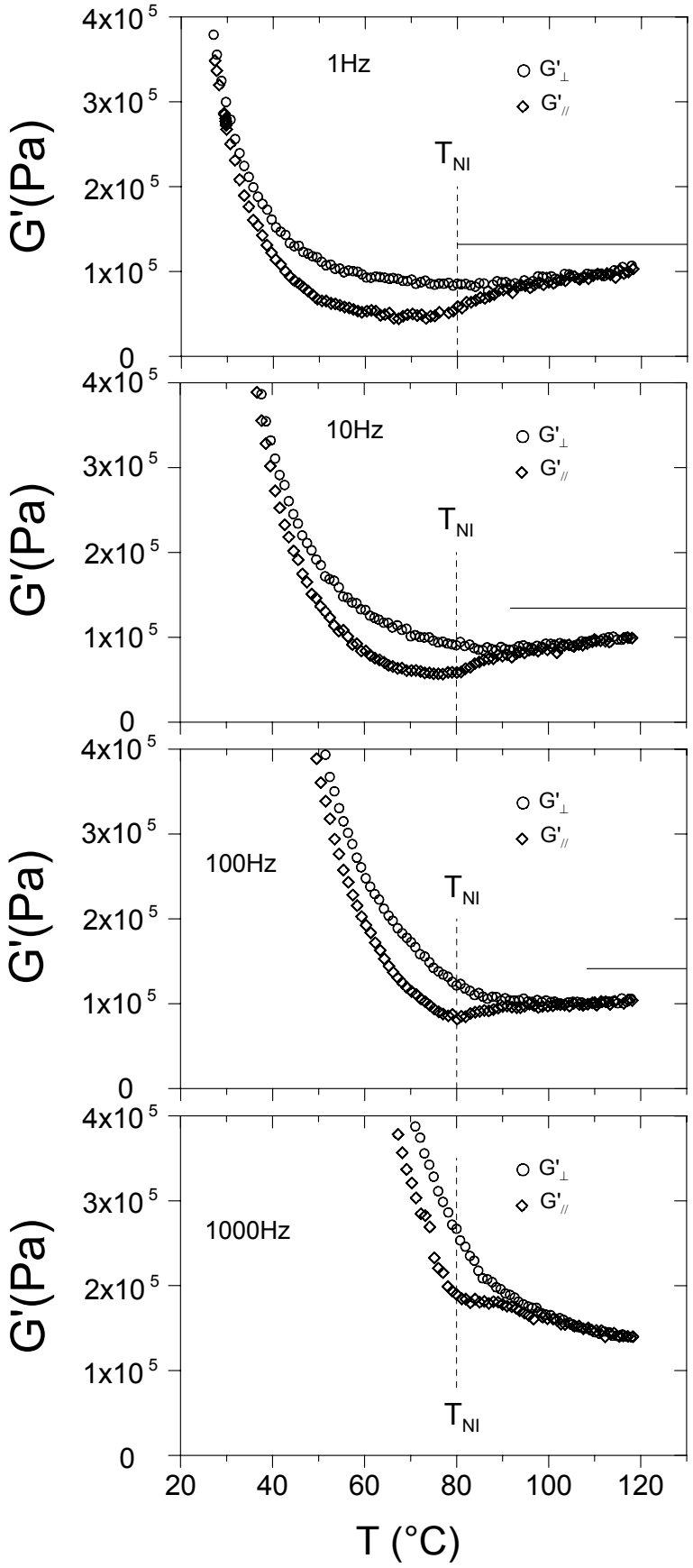
4x10^5
3x10^5
2x10^5
1x10^5
0
G'(Pa)
1Hz
10Hz
100Hz
1000Hz
G'⊥
G'//
T_NI
20
40
60
80
100
120
T (°C)

Fig. 6

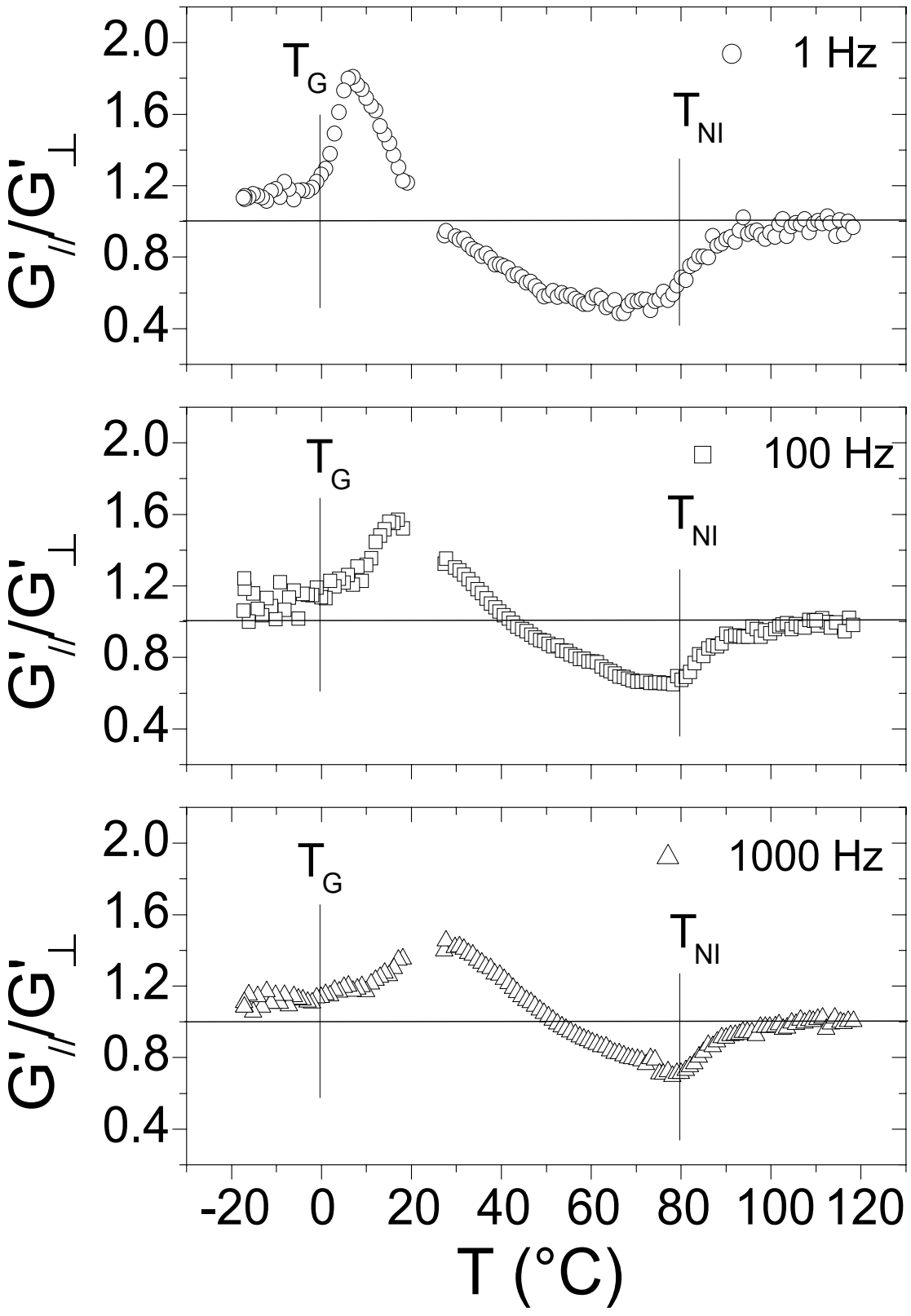
2.0
1.6
1.2
0.8
0.4
G'//G'⊥
T_G
T_NI
1 Hz
100 Hz
1000 Hz
-20
0
20
40
60
80
100
120
T (°C)

Fig. 7

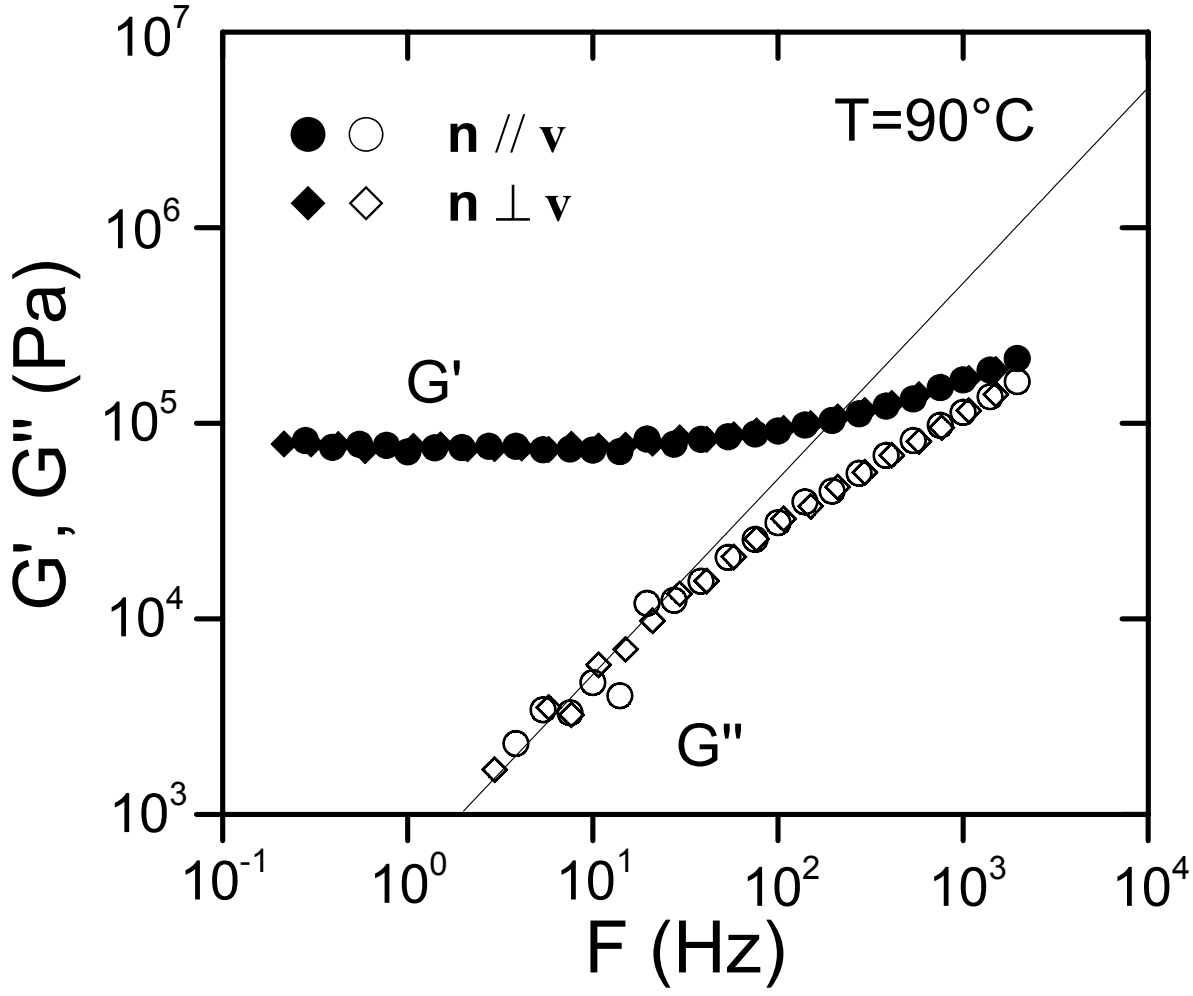
T=90°C
n // v
n ⊥ v
G'
G"
G', G" (Pa)
F (Hz)
10^7
10^6
10^5
10^4
10^3
10^-1
10^0
10^1
10^2
10^3
10^4

Fig. 8

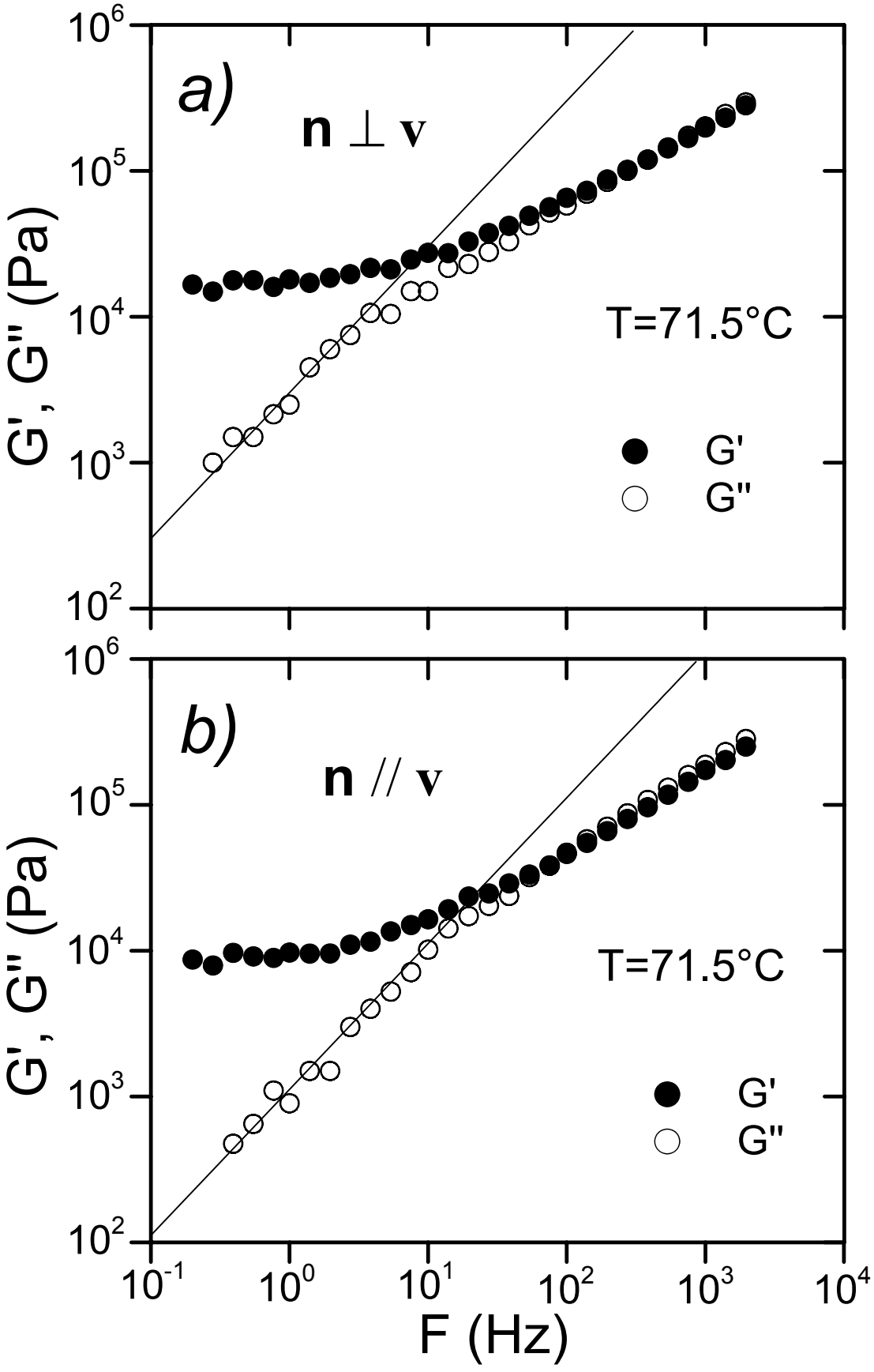
a)
n ⊥ v
T=71.5°C
G'
G"
b)
n // v
T=71.5°C
G'
G"
G', G" (Pa)
F (Hz)
10^6
10^5
10^4
10^3
10^2
10^-1
10^0
10^1
10^2
10^3
10^4

Fig. 9

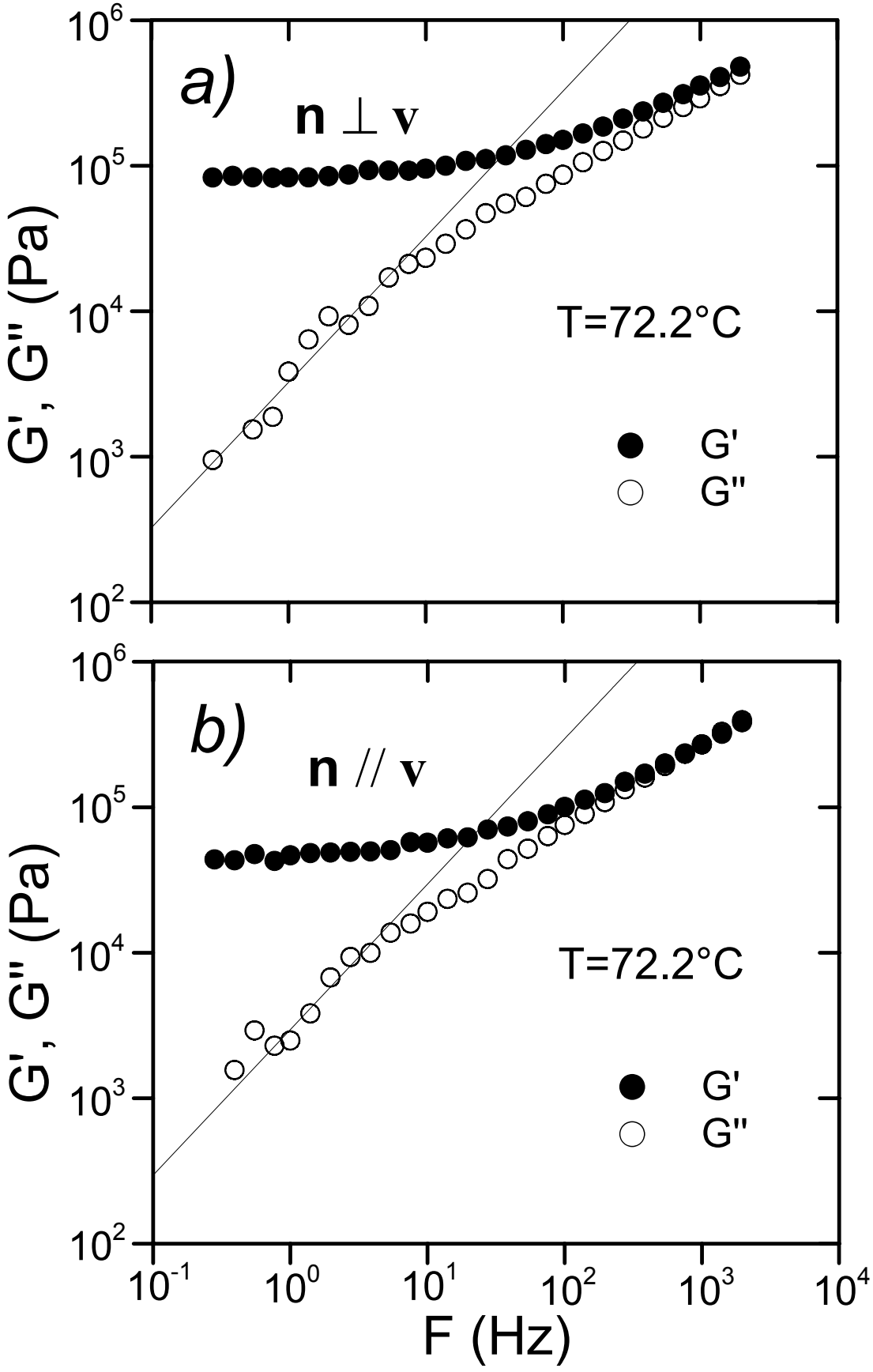

Fig. 10

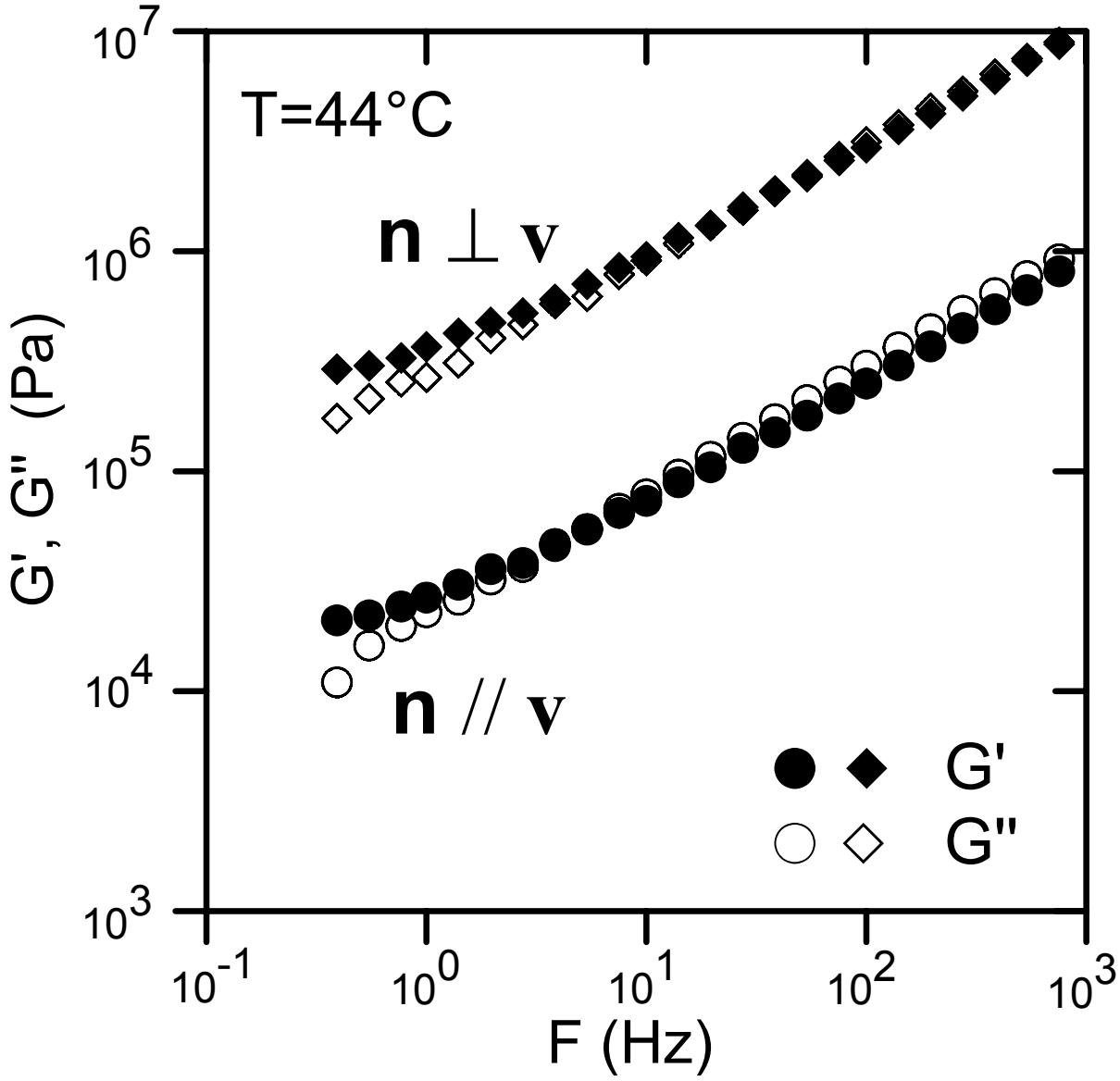

fig. 11